Sensors & Actuators: B. Chemical 408 (2024) 135530

Contents lists available at ScienceDirect

Sensors and Actuators: B. Chemical

journal homepage: www.elsevier.com/locate/snb

Capacitive model of enzyme-modified field-effect biosensors: Impact of enzyme coverage

Tobias Karschuck [a,b], Arshak Poghossian [c,*], Joey Ser [a], Astghik Tsokolakyan [d], Stefan Achtsnicht [a], Patrick Wagner [b], Michael J. Schöning [a,e,**]

[a] Institute of Nano- and Biotechnologies, FH Aachen, Heinrich-Mussmann-Str. 1, Jülich 52428, Germany
[b] Laboratory for Soft Matter and Biophysics, Department of Physics and Astronomy, KU Leuven, Celestijnenlaan 200 D, Leuven 3001, Belgium
[c] MicroNanoBio, Liebigstr. 4, Düsseldorf 40479, Germany
[d] Institute of Chemical Physics NAS RA, P. Sevak Str. 5/2, Yerevan 0014 , Armenia
[e] Institute of Biological Information Processing (IBI-3), Forschungszentrum Jülich GmbH, Wilhelm-Johnen-Str., Jülich 52425, Germany

ARTICLE INFO

Keywords:
Field-effect biosensor
Capacitive model
Enzyme coverage
Multianalyte detection
Penicillin
Urea

ABSTRACT

Electrolyte-insulator-semiconductor capacitors (EISCAP) belong to field-effect sensors having an attractive transducer architecture for constructing various biochemical sensors. In this study, a capacitive model of enzyme-modified EISCAPs has been developed and the impact of the surface coverage of immobilized enzymes on its capacitance-voltage and constant-capacitance characteristics was studied theoretically and experimentally. The used multicell arrangement enables a multiplexed electrochemical characterization of up to sixteen EISCAPs. Different enzyme coverages have been achieved by means of parallel electrical connection of bare and enzyme-covered single EISCAPs in diverse combinations. As predicted by the model, with increasing the enzyme coverage, both the shift of capacitance-voltage curves and the amplitude of the constant-capacitance signal increase, resulting in an enhancement of analyte sensitivity of the EISCAP biosensor. In addition, the capability of the multicell arrangement with multi-enzyme covered EISCAPs for sequentially detecting multianalytes (penicillin and urea) utilizing the enzymes penicillinase and urease has been experimentally demonstrated and discussed.

1. Introduction

Over the last years, field-effect chemical / biosensors, in particular, electrolyte-insulator-semiconductor capacitors (EISCAP), have attracted considerable interest due to their miniature sizes and weight, quick response, the ability for real-time and labeling-free detection as well as the possibility of cost-effective mass production using advanced micro- and nanotechnologies (see e.g., recent reviews [1–7]). Being in its primary transducer architecture a pH-sensitive device [7–9], EISCAPs selectivity towards other ions or molecules is typically obtained via modification of the gate surface with the appropriate chemo- or bio-recognition elements (receptors). This way, numerous EISCAP sensors were designed for the selective measurement of various ion concentrations [10–13], the electrostatic detection of biomolecules [14–20], viruses [21–23] as well as nanoparticles [24–26] by their charge, monitoring of polymer degradation [27], and the layer-by-layer deposition of polyions with alternating charge [28,29]. In addition, many enzyme-modified EISCAPs have been engineered for the analysis of diverse analytes (e.g., urea [30–33], glucose [31,32,34–36], creatinine [34,36,37], antibiotics [32,33,38–41], acetoin and diacetyl [42]) as well as for the design of enzyme-based logic gates (AND, OR, XOR, controlled NOT [33,43–45]), mimicking the operating principles of electronic logic gates.

Moreover, several attempts were made to develop on-chip integrated arrays of EISCAPs for multiplexed detection of multianalytes [46–48]. Generally, the benefits of multianalyte assay systems over biosensors for single-analyte recording include the reduced measurement time, lowered sample volume, high throughput and cost-effective assaying [49]. However, fabricating an array of individually addressable EISCAPs on the common silicon substrate (while excluding cross-talk between the sensors) requires complicated technological process steps. The consequence is a forfeiture of the essential advantages of EISCAPs, namely the

* Corresponding author.
** Corresponding author at: Institute of Nano- and Biotechnologies, FH Aachen, Heinrich-Mussmann-Str. 1, Jülich 52428, Germany.
E-mail addresses: a.poghossian@gmx.de (A. Poghossian), schoening@fh-aachen.de (M.J. Schöning).

https://doi.org/10.1016/j.snb.2024.135530
Received 17 November 2023; Received in revised form 14 February 2024; Accepted 20 February 2024
Available online 23 February 2024

simple structure and their easy and cost-efficient fabrication.

To overcome these drawbacks, we proposed recently a novel design for on-chip integration of an EISCAP array, capable of the multiplexed recording of multianalytes [50]. Beside the conventional sensing gate, each on-chip EISCAP structure contained a so-called control gate, which offers addressability of EISCAPs in terms of their activation or deactivation. This concept excludes any interference between the individual sensors, although they were still interconnected through a common silicon substrate. In an alternative approach, the surface of the EISCAP was separated into two spots, one immobilized with penicillinase and the other one with urease [32]. The multiplexing was achieved by consecutive exposure of the EISCAP gate to the buffer containing the corresponding substrate, i.e., penicillin or urea.

For both approaches, the receptor-covered spot area was significantly smaller than the entire surface area of the EISCAP chip contacting the analyte solution. A similar situation occurs when immobilized receptors (e.g., enzymes) only partially cover the EISCAP surface, resulting in a surface coverage η of $\eta < 1$. Owing to the working principle of a field-effect capacitor, the presence of receptor-free chip areas (here, defined as inactive) will result in an additional parasitic capacitance parallel to the capacitance of the receptor-covered areas (here, defined as active). As a consequence, a smaller signal contribution and reduced sensitivity of the sensor towards the analyte can be anticipated. This prediction was recently supported by EISCAPs modified with ligand-stabilized charged gold nanoparticles of different coverages [26]. The influence of the surface coverage of receptor layers (such as enzymes) on the EISCAP performance, however, still needs to be studied in detail.

In this work, a capacitive model for an enzyme-modified EISCAP biosensor was developed and the influence of enzyme surface coverage on the sensor signal has been studied theoretically and experimentally. The capacitance-voltage (C–V) curve and constant-capacitance (ConCap) signal of the EISCAP were simulated as a function of enzyme coverage. Bare and enzyme-modified EISCAPs were electrochemically characterized using a multicell arrangement, enabling the multiplexed addressing and readout of an array of up to 16 EISCAPs. Different enzyme coverages were accomplished via parallel electrical connection of bare and enzyme-modified single EISCAPs in various combinations. Finally, the ability of the multicell setup with multi-enzyme modified EISCAPs for the sequential detection of multianalytes without cross-talk effects was demonstrated experimentally and discussed. Penicillinase/penicillin and urease/urea were used as model enzyme/substrate systems, representing typical enzymatic reactions that generate H^+ or OH^- ions, respectively.

2. Capacitive model of enzyme-modified EISCAP biosensors

Enzyme-based EISCAP biosensors usually consist of an immobilized enzyme onto the gate surface of a pH-sensitive EISCAP [7]. Fig. 1a shows the schematic of such an EISCAP biosensor with a stacked double-insulator structure, partially covered with enzyme molecules.

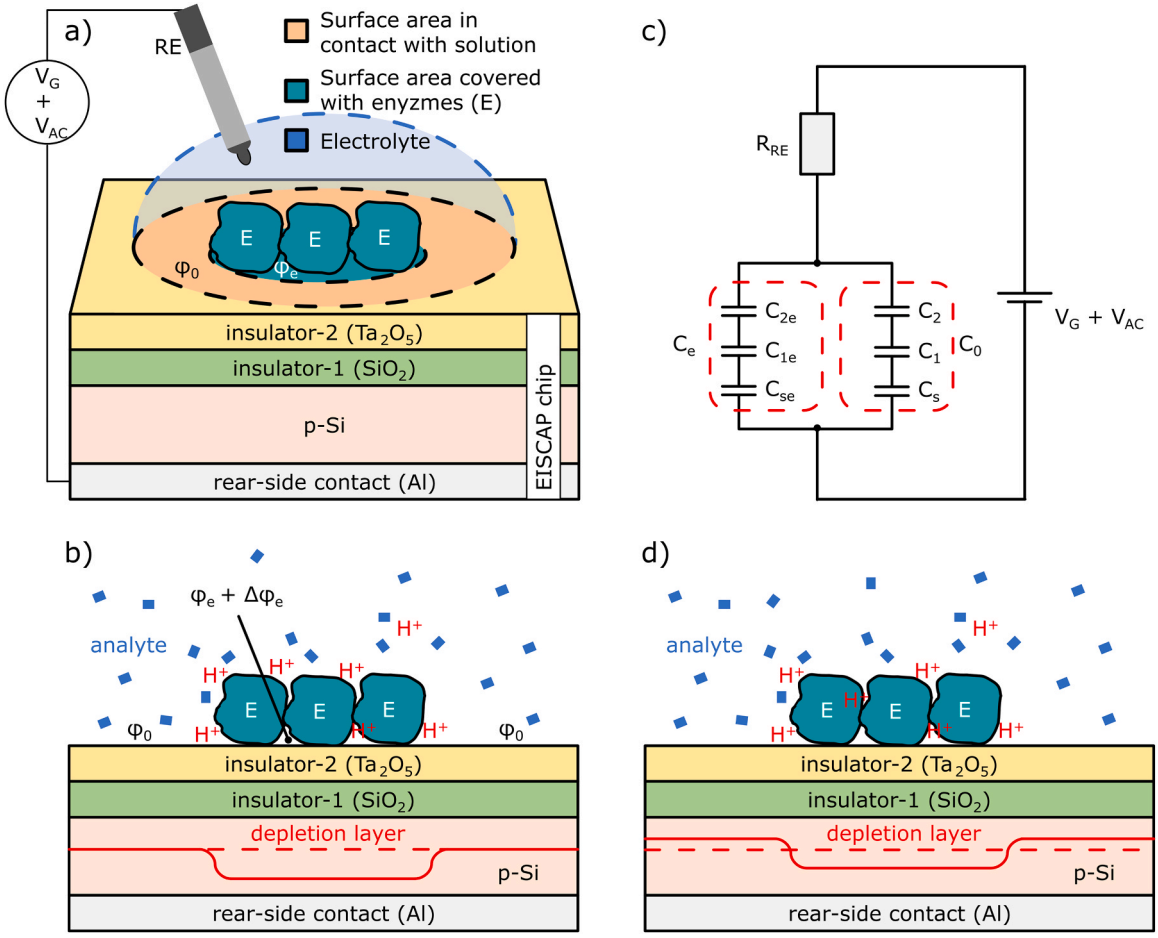

Fig. 1. Schematic structure of the EISCAP partially covered with enzymes (a), profile of the depletion layer during enzymatic reaction (b), electrical equivalent circuit (c), and profile of the depletion layer in p-Si at the gate voltage (V_{Ge}), which should be applied by the ConCap-mode measurement to maintain a constant working-point capacitance (d). The dashed lines in (b) and (d) indicate the width of the depletion layer in p-Si for the unmodified EISCAP at the gate voltage V_G. R_{RE}: reference-electrode resistance (RE); V_G: gate voltage; V_{AC}: alternating current voltage; C_{2e}, C_{1e}, C_{se}, C_e: gate-insulator-2, gate-insulator-1, space-charge and overall capacitance in the enzyme-covered region, respectively; C_2, C_1, C_s, C_0: gate-insulator-2, gate-insulator-1, space-charge and overall capacitance in the enzyme-free region, respectively; φ_e and φ_0: gate insulator-2/electrolyte interfacial potential in the enzyme-covered and enzyme-free regions, respectively.

The upper gate insulator-2 serves as the pH-sensitive layer (e.g., Ta_2O_5, Al_2O_3), whereas gate insulator-1 (typically, SiO_2) ensures stability of the oxide/semiconductor interface as it offers a low density of interface states. The surface area (A_e) covered with an enzyme layer is considered to be smaller than the total surface area (A) of the EISCAP chip contacting the electrolyte. Hence, enzyme surface coverage can be defined as $\eta = A_e/A$ (i.e., the enzyme-covered fraction of the EISCAP's surface contacting the solution). Thus, the model comprises the gate surfaces of EISCAPs with artificially patterned or partially immobilized enzyme areas as well as the surfaces with randomly immobilized enzymes, which form many small islands of active areas surrounded by inactive enzyme-free areas, all resulting in a surface coverage of $\eta < 1$. Since enzymes are typically charged in solutions, we assume that the immobilization of enzymes will locally alter the potential at the gate insulator-2/electrolyte interface. Thus, in a first approach, the EISCAP partially modified with enzymes can be divided into two regions:

1) an enzyme-free region with a surface area of $A_0 = A - A_e = A(1-\eta)$ and an interfacial potential of φ_0, and
2) an enzyme-covered region with a spot area of A_e, a surface coverage of η, and an interfacial potential of φ_e.

The operating principle of enzyme-based EISCAPs relies on the sensing of local pH variations caused by enzymatic reactions, which either generate H^+ ions (pH decrease) or consume H^+/generate OH^- ions (pH increase) [7]. Local changes in pH close to the surface of the pH-sensitive material will result in a modulation of the gate-surface charge, which, in turn, alters the width of the depletion region in the Si (see Fig. 1b). Accordingly, the space-charge capacitance in the Si and the total capacitance of the EISCAP will be modulated as well. The magnitude of the locally-induced pH variation and the amplitude of the recorded EISCAP signal are dependent on the concentration of the target analyte in solution. A large signal amplitude can be anticipated for EISCAPs with gate insulators displaying a high pH sensitivity (in this study, Ta_2O_5).

The C–V and ConCap method are two convenient modes for the electrochemical characterization of EISCAP biosensors [7,51]. The typical C–V curves reflect the well-known accumulation, depletion and inversion regions. For an EISCAP application as potential- and charge-sensitive device, the depletion region of the C–V plot is the usable range, where the total capacitance of the EISCAP is, among other parameters, a function of the gate voltage and the insulator/electrolyte interfacial potential [7]. Therefore, to define the influence of the enzyme coverage on the C–V characteristics, one should derive the equation for the equivalent capacitance of the enzyme-covered EISCAP in the depletion regime.

The simplified electrical equivalent circuit of the enzyme-modified EISCAP is presented in Fig. 1c. The resistances of the rear-side contact (Al-p-Si), bulk semiconductor and solution have not been included in the equivalent circuit, because they are usually negligible compared to the resistance (R_{RE}) of the reference electrode (RE). Moreover, for the gate-insulator thickness and measurement conditions used in this study, the double-layer capacitance at the gate insulator-2/electrolyte interface can be neglected [7,52,53]. Thus, the equivalent capacitance (C_{eq}) of the enzyme-based EISCAP can be expressed as a combination of the overall capacitances of the enzyme-covered (C_e) and enzyme-free (C_0) regions in parallel:

$$C_{eq} = C_e + C_0 \tag{1}$$

C_e is determined by the combination of the capacitances of insulator-2 (C_{2e}), insulator-1 (C_{1e}) and space-charge (C_{se}) in the enzyme-covered region in series:

$$\frac{1}{C_e} = \frac{1}{C_{2e}} + \frac{1}{C_{1e}} + \frac{1}{C_{se}} \tag{2}$$

where $C_{2e} = \varepsilon_2\varepsilon_0 A\eta/d_2 = A\eta C_{2a}$, $C_{1e} = \varepsilon_1\varepsilon_0 A\eta/d_1 = A\eta C_{1a}$, $C_{se} = \varepsilon_s\varepsilon_0 A\eta/w_{se} = A\eta C_{sea}$; ε_2, ε_1 and ε_s are the dielectric constants of insulator-2, insulator-1 and semiconductor, respectively; ε_0 is the vacuum permittivity, d_2 and d_1 are the thicknesses of insulator-2 and insulator-1, respectively, C_{2a} and C_{1a} are the capacitances of insulator-2 and insulator-1 per unit surface area, and w_{se} and C_{sea} are the depletion layer's width and capacitance (per unit area) for the enzyme-covered region.

The term C_0 in Eq. (1) is defined by the combination of the constant capacitances of insulator-2 (C_2), insulator-1 (C_1) and the variable space-charge capacitance (C_s) in the enzyme-free region in series:

$$\frac{1}{C_0} = \frac{1}{C_2} + \frac{1}{C_1} + \frac{1}{C_s} \tag{3}$$

where $C_2 = \varepsilon_2\varepsilon_0 A(1\text{-}\eta)/d_2 = A(1\text{-}\eta)C_{2a}$, $C_1 = \varepsilon_1\varepsilon_0 A(1\text{-}\eta)/d_1 = A(1\text{-}\eta)C_{1a}$, $C_s = \varepsilon_s\varepsilon_0 A(1\text{-}\eta)/w_s = A(1\text{-}\eta)C_{sa}$; w_s and C_{sa} are the depletion layer's width and capacitance (per unit area) for the enzyme-free region.

Generally, the depletion capacitance per unit surface area for an EISCAP with a stacked double-insulator structure is given by [50,54]:

$$C_a = \frac{1}{\sqrt{\left(\frac{C_{1a}+C_{2a}}{C_{1a}C_{2a}}\right)^2 + \frac{2\left(V_G - V_{fb}\right)}{qN_A\varepsilon_s}} - \frac{C_{1a}+C_{2a}}{C_{1a}C_{2a}}} \tag{4}$$

In expression (4), V_G is the gate voltage, q is the elementary charge (1.6×10^{-19} C), N_A is the density of ionized acceptors and V_{fb} represents the flat-band voltage given by [50]:

$$V_{fb} = V_{ip} - \varphi \tag{5}$$

where φ is the interfacial potential and V_{ip} represents a group of analyte-concentration independent potentials. By assuming that the charges located in the stacked insulators and the surface and interface states are zero, V_{ip} can be determined as [50]:

$$V_{ip} = E_{ref} + \chi_{sol} - W_s/q \tag{6}$$

Here, E_{ref} represents the potential of the RE relative to vacuum, χ_{sol} is the surface-dipole potential of the solvent and W_s is the silicon electron work function. The expressions for C_{sea} and C_{sa} can be obtained by replacing the term φ in Eq. (5) with the interfacial potentials corresponding to the enzyme-covered (φ_e) and enzyme-free (φ_0) regions, respectively, and subsequent substitution in Eq. (4). Hence, C_{se} and C_s can be expressed as:

$$C_{se} = A\eta C_{sea} = \frac{A\eta}{\sqrt{\left(\frac{C_{1a}+C_{2a}}{C_{1a}C_{2a}}\right)^2 + \frac{2\left(V_G - V_{ip} + \varphi_e\right)}{qN_A\varepsilon_s}} - \frac{C_{1a}+C_{2a}}{C_{1a}C_{2a}}} \tag{7}$$

$$C_s = A(1-\eta)C_{sa} = \frac{A(1-\eta)}{\sqrt{\left(\frac{C_{1a}+C_{2a}}{C_{1a}C_{2a}}\right)^2 + \frac{2\left(V_G - V_{ip} + \varphi_0\right)}{qN_A\varepsilon_s}} - \frac{C_{1a}+C_{2a}}{C_{1a}C_{2a}}} \tag{8}$$

The potential (φ_0) at the interface electrolyte/pH-sensitive gate-insulator-2 is given by [55–57]:

$$\varphi_0 = 2.3\frac{kT}{q}\alpha\left(pH_{pzc} - pH\right) \tag{9}$$

where k is the Boltzmann's constant, T is the temperature of solution (in K), pH_{pzc} represents the pH value at the point of zero charge (PZC), and $\alpha = S/S_{Nernst}$ is a dimensionless sensitivity parameter (between 0 and 1), representing the real sensitivity (S) of the used pH-sensitive gate insulator relative to the ideal Nernstian sensitivity ($S_{Nernst} \approx 59.16$ mV/pH at room temperature (RT), $T_0 = 298$ K).

The equation for the equivalent capacitance of the enzyme-covered EISCAP in the depletion region is obtained by substitution of Eqs. (2), (3), (7) and (8) into Eq. (1):

$$C_{eq} = \frac{A\eta}{\sqrt{\left(\frac{C_{1a}+C_{2a}}{C_{1a}C_{2a}}\right)^2 + \frac{2(V_G - V_{ip} + \varphi_e)}{qN_A\varepsilon_s}}} + \frac{A(1-\eta)}{\sqrt{\left(\frac{C_{1a}+C_{2a}}{C_{1a}C_{2a}}\right)^2 + \frac{2(V_G - V_{ip} + \varphi_0)}{qN_A\varepsilon_s}}} \quad (10)$$

When the enzyme-modified EISCAP chip is exposed to the analyte solution, local pH variations (ΔpH) caused by the enzyme/substrate reaction nearby the gate surface of the enzyme-covered region will result in an analyte-concentration (c) dependent change ($\Delta\varphi_e = f(c)$) in the electrolyte-insulator interfacial potential. This can be deduced from Eq. (9):

$$\Delta\varphi_e = -2.3\frac{kT}{q}\alpha\Delta pH \quad (11)$$

Here, $\Delta pH = f(c)$ is dependent on the substrate concentration. By assuming that the enzymatic reaction occurs only in the enzyme-covered region of the EISCAP chip and, to a first approximation, neglecting the possible influence of lateral diffusion of generated protons or hydroxide ions to the enzyme-free region, the equivalent capacitance ($C_{eq\text{-}c}$) in the depletion range (in the presence of analyte) will be determined as:

$$C_{eq-c} = \frac{A\eta}{\sqrt{\left(\frac{C_{1a}+C_{2a}}{C_{1a}C_{2a}}\right)^2 + \frac{2(V_G - V_{ip} + \varphi_e \pm \Delta\varphi_e)}{qN_A\varepsilon_s}}} + \frac{A(1-\eta)}{\sqrt{\left(\frac{C_{1a}+C_{2a}}{C_{1a}C_{2a}}\right)^2 + \frac{2(V_G - V_{ip} + \varphi_0)}{qN_A\varepsilon_s}}} \quad (12)$$

where the terms $+\Delta\varphi_e$ or $-\Delta\varphi_e$ correspond to the enzymatic reactions producing H^+ or OH^- ions, respectively.

Eqs. (10) and (12) render the shape of the C–V plot of the enzyme-modified EISCAP in the depletion range before and during the enzymatic reaction. The evaluation of Eq. (12) shows that, at a constant V_G, the equivalent capacitance ($C_{eq\text{-}c}$) in the presence of the analyte depends, among other parameters, on the enzyme coverage (η) and analyte-concentration dependent potential change ($\Delta\varphi_e$) at the electrolyte/gate-insulator-2 interface (induced by the local pH variation due to the enzymatic reaction).

Besides the C–V plot, the influence of the enzyme coverage on the amplitude of the ConCap signal of the enzyme-covered EISCAP is also very important. Note that, in the ConCap mode, the working capacitance is kept at a fixed value by applying an instantly sign-inverted gate voltage to the EISCAP structure via a feedback circuit [7]. The gate voltage (V_{Ge}), which is necessary to apply in order to maintain a constant working capacitance of the enzyme-covered EISCAP, can be deduced from Eqs. (10) and (12) under the condition that $C_{eq\text{-}c} = C_{eq}$:

$$\frac{\eta}{\sqrt{\left(\frac{C_{1a}+C_{2a}}{C_{1a}C_{2a}}\right)^2 + \frac{2(V_{Ge} - V_{ip} + \varphi_e \pm \Delta\varphi_e)}{qN_A\varepsilon_s}}} + \frac{1-\eta}{\sqrt{\left(\frac{C_{1a}+C_{2a}}{C_{1a}C_{2a}}\right)^2 + \frac{2(V_{Ge} - V_{ip} + \varphi_0)}{qN_A\varepsilon_s}}} = \frac{\eta}{\sqrt{\left(\frac{C_{1a}+C_{2a}}{C_{1a}C_{2a}}\right)^2 + \frac{2(V_G - V_{ip} + \varphi_e)}{qN_A\varepsilon_s}}} + \frac{1-\eta}{\sqrt{\left(\frac{C_{1a}+C_{2a}}{C_{1a}C_{2a}}\right)^2 + \frac{2(V_G - V_{ip} + \varphi_0)}{qN_A\varepsilon_s}}} \quad (13)$$

The profile of the depletion layer in the Si underneath enzyme-covered and enzyme-free regions at the gate voltage (V_{Ge}) applied by the ConCap-mode measurements is schematically presented in Fig. 1d.

We simulated C–V plots in the depletion range and the ConCap signal change ($\Delta V_{Ge} = V_G - V_{Ge}$) of an EISCAP as a function of the enzyme coverage in the presence of the analyte by Eqs. (12) and (13) using Python 3.9. We applied the following parameters for the simulation: $\varepsilon_0 = 8.854 \times 10^{-12}$ F/m, $\varepsilon_1 = 3.9$ (SiO_2), $\varepsilon_2 = 25$ (Ta_2O_5), $\varepsilon_s = 11.7$ (Si), $d_1 = 30$ nm, $d_2 = 60$ nm, $N_a = 6.2 \times 10^{15}$ cm^{-3}, $q = 1.6 \times 10^{-19}$ C, $k = 1.38 \times 10^{-23}$ J/K, $A = 2$ cm^2, $V_{ip} = 0$ V, $\varphi_0 = -10$ mV, $\varphi_e = -50$ mV, $\Delta\varphi_e = 60$ mV, $T = 300$ K, and $\eta = 0$, 0.25, 0.5, 0.75, and 1.

Fig. 2a depicts simulated C–V plots in the depletion range for a p-type EISCAP modified with enzymes of different coverages. At constant values of V_G and $\Delta\varphi_e$, the local pH decrease (here, assuming an enzymatic reaction producing H^+ ions) on the enzyme-covered surface region will decrease the total capacitance of the EISCAP. As a consequence, the C–V plots move along the gate-voltage axis towards less positive voltages. The higher the enzyme coverage, the larger is the shift of the C–V curves.

ConCap signal changes (i.e., the additional gate voltage $\Delta V_{Ge} = V_G - V_{Ge}$, required to maintain a constant working capacitance of the enzyme-covered EISCAP biosensor) on the enzyme coverage was simulated with Eq. (13) and is illustrated in Fig. 2b. Noticeably, as the enzyme coverage increases from $\eta = 0.25$ to $\eta = 1$, ΔV_{Ge} increases from 16 mV to 60 mV.

It should be mentioned that Eqs. (12) and (13) do not take into account possible lateral diffusion of generated protons or hydroxide ions from the enzyme-covered to the enzyme-free region [58]. To consider the impact of lateral diffusion of produced ions on the described capacitive model as well as on the EISCAP signal, the capacitance of the diffusion region with the surface-potential profile (corresponding to the diffusion profile of H^+ or OH^- ions) must be included in Eqs. (12) and (13). For this, Fick's equation can be used to describe the spatiotemporal concentration distribution of produced ions in the diffusion region.

It should be pointed out that the presented capacitive model can also be extended to EISCAP biosensors modified with multi-enzymes for the successive detection of multiple analytes.

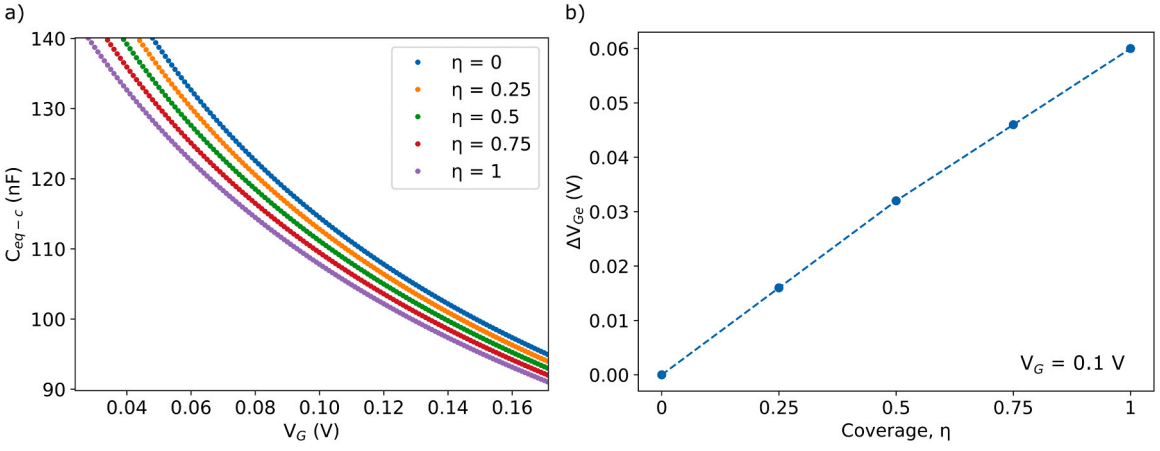

Fig. 2. (a) Simulated C–V plots in the depletion range (in the presence of the analyte) for a p-type EISCAP modified with enzymes of different coverages. (b) Calculated ConCap signal change ($\Delta V_{Ge} = V_G - V_{Ge}$) of an enzyme-modified EISCAP as a function of the enzyme coverage varying from $\eta = 0$ to $\eta = 1$.

3. Experimental

3.1. Fabrication of the Ta_2O_5-gate EISCAPs

EISCAPs composed of an Al-p-Si-SiO_2-Ta_2O_5 layer structure with chip sizes of 1 cm × 1 cm were fabricated from commercially available p-Si-SiO_2 wafers (Siegert Wafer, Germany) with a 30 nm SiO_2 film prepared by dry thermal oxidation of a p-Si substrate (thickness: 380 ± 15 µm, specific resistivity: 5 – 10 Ωcm). As a pH-sensitive gate insulator we used Ta_2O_5, which is one of the best pH-sensitive materials possessing a nearly-Nernstian pH sensitivity, low hysteresis and small drift rate [7–9,59]. The 60 nm thick Ta_2O_5 film was fabricated on the SiO_2 layer via electron-beam evaporation of a 30 nm Ta layer and subsequent dry thermal oxidation in O_2 atmosphere at 520 °C for 2 h, according to the protocol given in [60]. Afterwards, the back-side of the SiO_2 layer was etched with 5% HF, followed by electron-beam evaporation of 300 nm Al as contact layer and annealing in N_2 atmosphere at 400 °C for 10 min. After dicing the wafer, the fabricated EISCAP chips were cleaned in an ultrasonic bath with acetone, isopropanol, ethanol, and deionized water for 3 min each, followed by drying with N_2. The cleaned EISCAPs were installed into a custom-built multicell and sealed by a Viton O-ring to protect the side walls of the chips and the Al rear-side contacts from the solution. The remaining surface area of the Ta_2O_5 gate in contact with the solution was approximately 50 mm^2. Before multiplexed electrochemical characterization, the EISCAPs installed in the multicell, see Fig. 3, were conditioned at RT overnight in pH 7 Titrisol buffer (Merck, Germany).

3.2. Multicell design and measurement setup

The bare and enzyme-modified EISCAPs were electrochemically characterized using the impedance analyzer Zahner IM6ex (Zahner Elektrik, Germany). The setup enables multiple addressing and readout of an array of 16 sensors installed in the multicell arrangement having one common RE. From the center of the multicell, where the RE (Metrohm, Germany) was mounted, fluidic channels connect to the sensor reservoirs, which are all located at the same distance from the RE (see Fig. 3a, where the position of EISCAPs in the multicell is indicated, too). A custom Python script, build upon Zahner Elektrik's GitHub repository [61], can was utilized for the multiplexing and fully automatic characterization of 16 EISCAP biosensors in the $C-V$ and ConCap modes. The benefits of the multicell arrangement used in this study include [62]: i) the ability to characterize not only single EISCAPs, but also a group of parallel-connected EISCAPs with various combinations of bare and enzyme-modified EISCAPs, thus, mimicking the variation of enzyme surface coverage; ii) a fully automated multiplexed characterization of up to 16 EISCAPs by using only one conventional reference electrode to ensure comparability of the measurement results and cost-effectiveness; iii) the possibility of an immobilization of different enzymes on different EISCAP surfaces at the same time, making the system highly versatile for many applications; iv) an interchangeable, and nondestructive installation and dismounting of the EISCAPs as well as easy integration of the multicell arrangement with the impedance analyzer; v) the possibility of differential-mode measurements. Moreover, the distance between neighboring EISCAPs in the multicell was sufficiently large (approximately 13 mm) in order to practically exclude any cross-talk effects caused via the possible lateral diffusion of H^+ or OH^- ions generated by the enzymatic reactions during the measurement routine.

Fig. 3b shows a photo of the fully assembled multicell arrangement with cover plate and mounted RE. More details on the multiplexing system and multicell design can be found in ref. [62].

For characterizing the EISCAPs in the $C-V$ mode, a direct-current (DC) gate voltage (from −2 V to 2 V in 100 mV increments) and a superimposed alternating-current (AC) voltage (20 mV with a frequency of $f = 120$ Hz) was applied between the RE and the rear-side Al contact of either the preselected single EISCAP in the array or a group of parallel-connected EISCAPs. After recording of the $C-V$ curve, the working point (i.e., the constant capacitance) for the time-resolved measurement of the ConCap response was arranged by the Python script within the $C-V$ curve's quasi-linear range (usually, at ~60% of the measured maximum capacitance in the accumulation range [7,62]). Here, the total capacitance of the EISCAP is more sensitive to potential variations. For multiplexed ConCap measurements, the signal of each EISCAP has been recorded consecutively for 2 s, beginning with EISCAP-1 and continuing to EISCAP-16. This cycle has been repeated during the typical ConCap measurement time of about 10 min. All measurements have been conducted at room temperature in a dark and grounded Faraday box to protect the EISCAP biosensor from the effects of ambient light and/or electromagnetic fields.

3.3. Enzyme immobilization and preparation of penicillin and urea solutions

Enzyme solutions were prepared by dissolving penicillinase

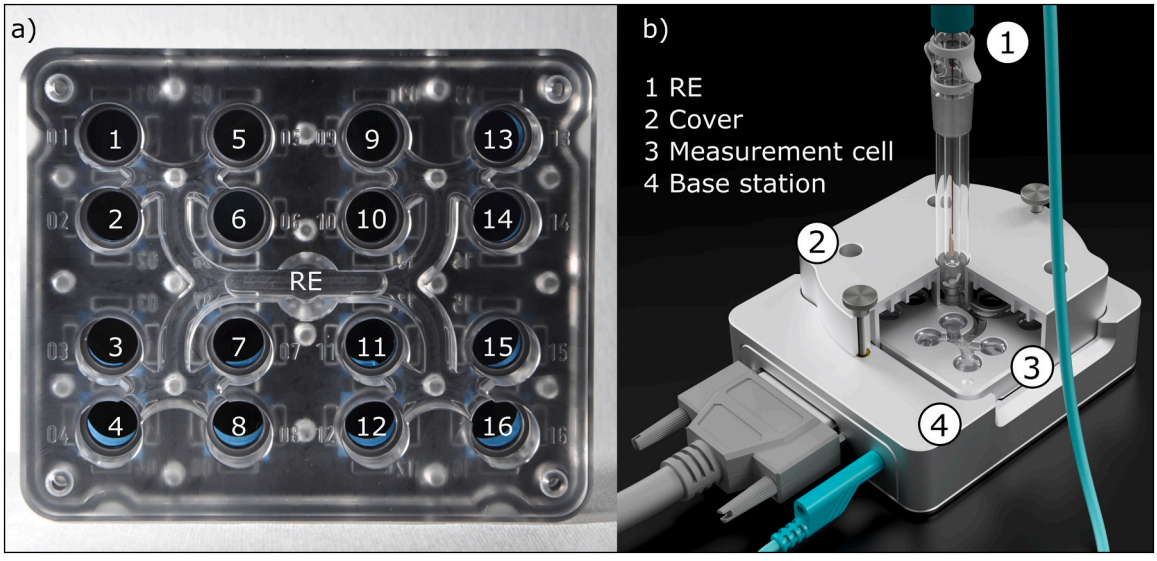

Fig. 3. Position of sixteen EISCAPs and RE in the multicell (a) and fully assembled multicell arrangement with cover plate and mounted RE (b). RE: reference electrode.

(*β*-lactamase from *Bacillus cereus* with a specific activity of about 2000 U/mg protein, Sigma-Aldrich, Germany) or urease (from Jack bean, *Canavalia ensiformis*, specific activity of about 76 U/mg solid, Sigma-Aldrich, Germany) in 1×PBS (phosphate buffered saline), pH 7.4. The enzymes penicillinase and urease were adsorptively immobilized on the gate surface of the EISCAPs. For the immobilization, 50 µl of the penicillinase (30 U) or urease (100 U) solution was drop-coated onto the Ta_2O_5 layer of the selected single EISCAPs and incubated at RT for about 2 h in a humid chamber. Finally, the sensors were rinsed with 0.33 mM PBS, pH 7.4 (further referred to as measurement buffer) and dried at RT. When not in use, the enzyme-modified EISCAPs were stored in a measurement buffer at 4 °C.

Penicillin and urea solutions have been prepared by adding penicillin G (Sigma–Aldrich, Germany) or urea (Fluka Analytical, Germany) to the measurement buffer. The pH value of the prepared penicillin and urea solutions was comparable to the optimal pH working range reported for penicillinase [63] and urease [64].

4. Results and discussion

4.1. Electrochemical characterization of single EISCAPs: leakage current and pH sensitivity

The gate leakage current level is an essential factor determining the correct functioning of EISCAPs. High leakage currents indicate a defective/degraded gate insulator. As a consequence, the EISCAPs may lose their functionality. Therefore, the gate-leakage current of all blank EISCAPs has been tested to ensure the quality of the gate insulator consisting of a stacked SiO_2-Ta_2O_5 double layer. The leakage current of each EISCAP has been recorded in pH 7 Titrisol buffer (Merck, Germany) by applying gate voltages between −2 V and +2 V. Only EISCAPs with a small leakage current below 10 nA were utilized for additional $C-V$ and ConCap characterization as well as for enzyme immobilization; for the majority of tested EISCAPs, the maximum leakage current was < 6 nA.

Since the output signal of enzyme-modified EISCAP biosensors depends on the local pH changes caused by the enzyme/substrate reaction (here, penicillinase/penicillin or urease/urea), the pH sensitivity of bare Ta_2O_5-gate EISCAPs has been evaluated from the $C-V$- and ConCap-mode measurements. The experiments were conducted in Titrisol buffer solutions with various pH values between pH 5 and pH 9. All $C-V$ curves had an identical shape with characteristic accumulation, depletion and inversion ranges.

The ConCap signal was recorded in the pH loop of 7 → 6 → 5 → 6 → 7 → 8 → 9 → 8 → 7 and also demonstrated a clear pH dependence. The mean pH sensitivity of sixteen bare EISCAPs in the multicell with Ta_2O_5 as pH-sensitive layer was about 59 mV/pH, which agrees well with the literature values reported for different types of Ta_2O_5-gate field-effect pH sensors (see e.g., [8,9,65–67]). The evaluated pH sensitivity of

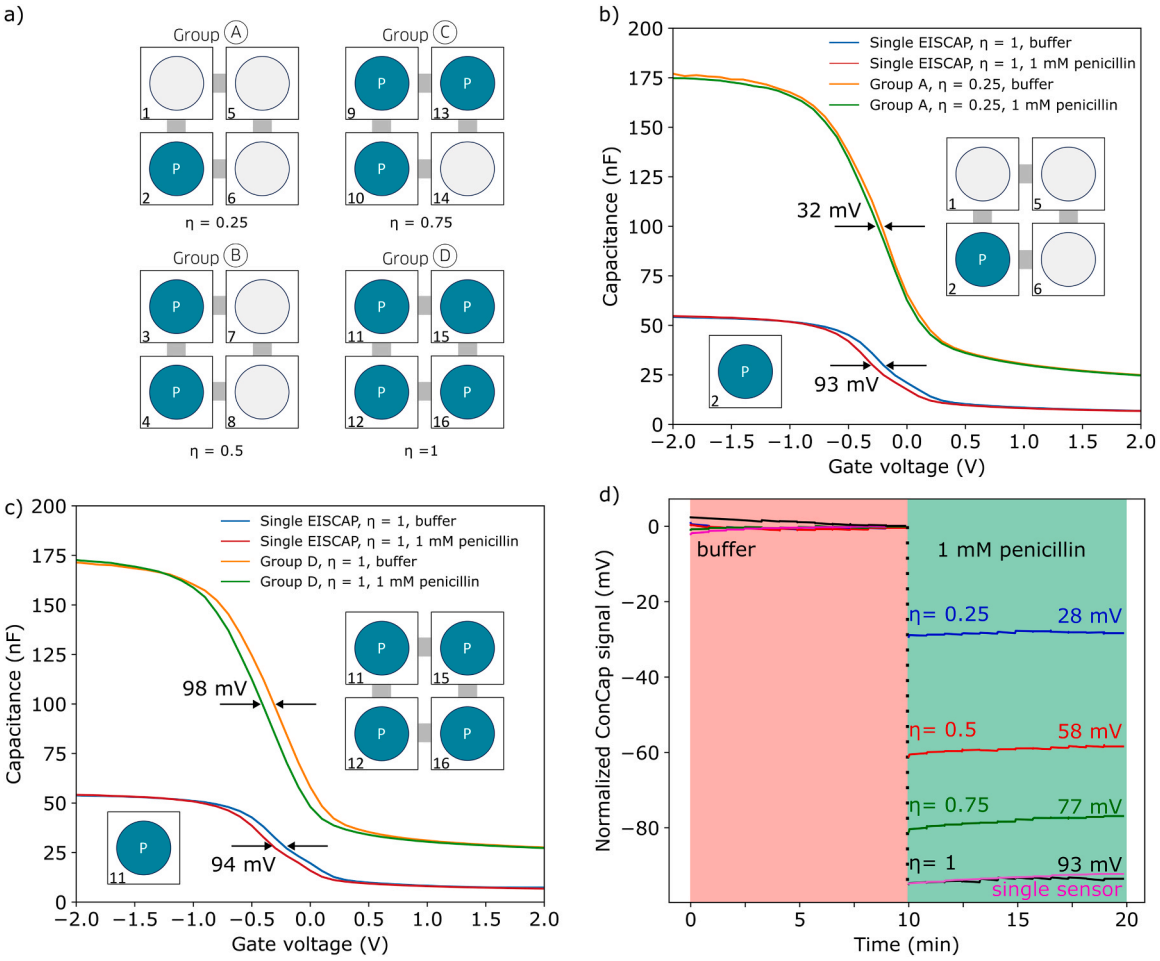

Fig. 4. (a) Combinations of bare and/or penicillinase-modified EISCAPs in groups A, B, C and D. The electrical connections are depicted as gray lines. (b) $C-V$ curves of parallel-connected EISCAPs in group A with a penicillinase coverage of $\eta = 0.25$. (c) $C-V$ curves of parallel-connected EISCAPs in group D with a penicillinase coverage of $\eta = 1$. (d) Normalized ConCap signals of parallel-connected EISCAPs in groups A, B, C and D, corresponding to a penicillinase coverage of $\eta = 0.25$, 0.5, 0.75, and 1, respectively. For comparison, (b) and (c) also show the $C-V$ plots of the penicillin-modified single EISCAPs (EISCAP-2 in group A and EISCAP-11 in group D) with an enzyme coverage of $\eta = 1$, and the normalized ConCap signal of a single EISCAP-11 (pink) is included in (d). All measurements were performed in buffer and in 1 mM penicillin solution. P: penicillinase.

EISCAPs will be used in Section 4.2 to estimate the local pH change onto the EISCAP surface caused from the enzymatic reaction. For exemplary data of $C-V$ and ConCap measurements on a bare EISCAP sensor, see Supplementary Information, Fig. S1.

4.2. Characterization of penicillinase-modified EISCAPs: impact of enzyme coverage

Enzymes were immobilized on the complete gate surface of selected single EISCAPs in contact with the solution (i.e., the enzyme coverage of these modified single EISCAPs can be considered as 100% or $\eta = 1$). To study the influence of enzyme coverage on the EISCAP signal in analyte solution, sixteen EISCAPs in the multicell were divided in four groups (A, B, C, and D) with various combinations of bare and/or penicillinase-modified EISCAPs, see Fig. 4a. For example, group A combined three bare (unmodified) EISCAPs and one penicillinase-modified EISCAP, while group D consisted of four penicillinase-modified single EISCAPs. Hence, different enzyme coverages were achieved by parallel electrical connection of four single EISCAPs (via short-circuiting the rear-side contacts; see gray lines in the figure) in each group. These parallel-connected single EISCAPs could be considered as one "large" EISCAP having a four times larger gate-surface area contacting the electrolyte. This way, different penicillinase coverages of $\eta = 0.25$ (group A), 0.5 (group B), 0.75 (group C) and 1 (group D) with a good reproducibility can be easily achieved, using the multicell arrangement described in Section 3.2.

The exemplary $C-V$ curves of parallel-connected EISCAPs in groups A and D, corresponding to the penicillinase coverage of $\eta = 0.25$ and $\eta = 1$, are presented in Figs. 4b and 4c, respectively. The measurements were conducted in buffer and in 1 mM penicillin solution. For comparison, Figs. 4b and 4c represent also the $C-V$ plots of the penicillin-modified single EISCAPs (EISCAP-2 in group A and EISCAP-11 in group D) with a coverage of $\eta = 1$.

As expected, in the presence of penicillin in buffer, the $C-V$ plots have shifted towards more negative voltages, which conforms to a more positively charged gate surface. Such a shift of $C-V$ plots is attributed to the local increase of H^+-ion concentration (i.e., pH decrease) near the enzyme-covered Ta_2O_5 surface induced by the penicillinase-catalyzed hydrolysis of penicillin (see e.g., [7]):

$$\text{penicillin} + H_2O \xrightarrow{\text{penicillinase}} \text{penicilloic acid} + H^+ \quad (14)$$

At a constant penicillin concentration of 1 mM, a small voltage shift of 32 mV has been registered for the parallel-connected EISCAPs (group A) with an enzyme coverage of $\eta = 0.25$ (Fig. 4b), while large voltage shifts of 93 − 94 mV and 98 mV were observed for the single (EISCAP-2 and EISCAP-11) and parallel-connected EISCAPs (group D), respectively, both with an enzyme coverage of $\eta = 1$ (Fig. 4c).

Fig. 4d depicts the normalized ConCap signals of parallel-connected EISCAPs in groups A, B, C and D, corresponding to the penicillinase coverage of $\eta = 0.25$, 0.5, 0.75, and 1. The ConCap signals show a clear dependence on enzyme coverage that supports the simulation results given in Section 2. With increasing enzyme coverage from $\eta = 0.25$ to $\eta = 1$, the ConCap signal raised from 28 mV to 93 mV. As anticipated, the ConCap signal's amplitude changes recorded for a single EISCAP-11 (pink) and four parallel-connected EISCAPs (group D, black) with an enzyme coverage of $\eta = 1$ was practically identical with a value of about 93 mV. Considering a pH sensitivity of 59 mV/pH for our EISCAPs (see Section 4.1), the ConCap signal change of 93 mV corresponds to a local pH decrease by approximately $\Delta pH \approx 1.6$.

To assess the effect of the enzyme coverage on the penicillin sensitivity, the ConCap signal of parallel-connected EISCAPs in the groups B, C, and D (corresponding to a penicillinase coverage of $\eta = 0.5$, 0.75, and 1) were measured at various penicillin concentrations between 0.2 mM and 2 mM. As can be seen in Fig. 5a, at all penicillin concentrations, the normalized ConCap signals show a clear dependence on enzyme coverage. The calibration plots of the EISCAP penicillin biosensors, determined from the ConCap curves in Fig. 5a at different enzyme coverages, are given in Fig. 5b. With increasing enzyme coverage from $\eta = 0.5$ to $\eta = 1$, the penicillin sensitivity of the EISCAPs rose from 42 mV/dec to 70 mV/dec.

The obtained results show that, owing to the working principle of field-effect EISCAPs, the presence of inactive (i.e., without or partially immobilized enzyme) areas of the chip surface in contact with solution will result in additional parasitic capacitances parallel to the capacitance of the active (i.e., with immobilized enzyme) chip region. The consequence is a smaller output signal and a reduced analyte sensitivity.

As indicated in Section 3.2, the minimum distance between neighboring EISCAPs in the multicell was sufficiently large (~13 mm) in order to practically exclude possible cross-talk effects due to the lateral diffusion of H^+ or OH^- ions produced by the enzymatic reactions. However, in a real situation, if the separation between the enzyme (penicillinase)-covered active and enzyme-free passive areas of the EISCAP surface is small (or even is zero), part of the H^+ ions, produced via the penicillinase/penicillin reaction, will laterally diffuse from the penicillinase-covered active region to the neighboring enzyme-free passive region (in addition to diffusion of H^+ ions to the bulk solution perpendicular to the EISCAP surface). As a consequence, the surface

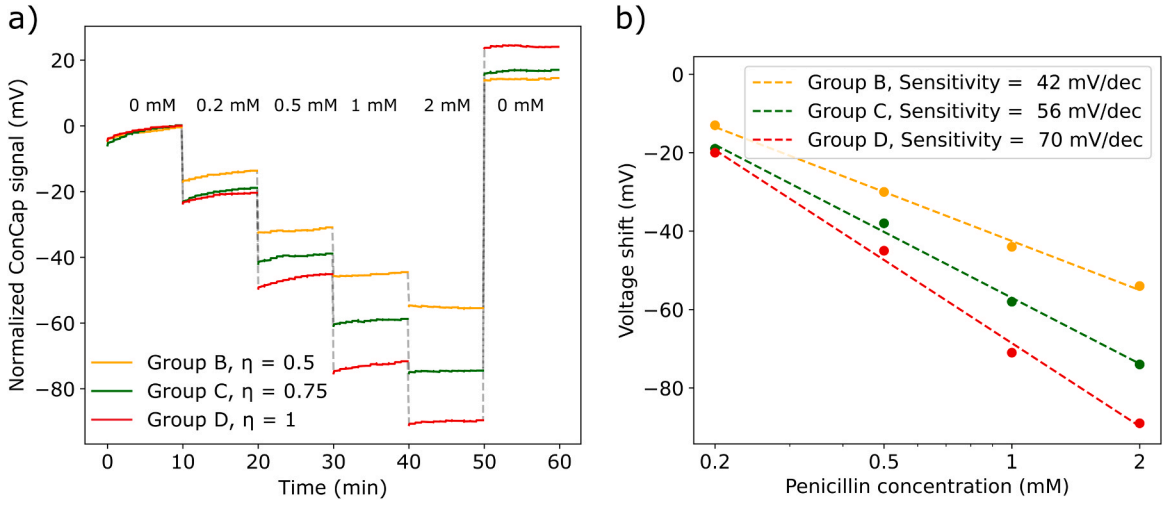

Fig. 5. Normalized ConCap signals of parallel-connected EISCAPs (groups B, C and D) with different penicillinase coverage of $\eta = 0.5$, 0.75, and 1, recorded at various penicillin concentrations between 0.2 mM and 2 mM (a) and corresponding calibration plots (b).

potential and capacitance in the diffusion region (i.e., the transition region from enzyme-covered to enzyme-free spot) will be changed to some extent. At the same time, the surface potential and the capacitance in the remaining enzyme-free passive region (outside of the diffusion region) will not change. Similar diffusion effects of produced ions will occur if the EISCAP surface is divided into two spots modified with two different enzymes (e.g., penicillinase and urease).

In the literature, lateral diffusion lengths between 100 μm and 1 mm (depending on experimental conditions) were reported for protons produced by enzymatic reactions or water electrolysis, studied by means of light-addressable sensors (see e.g., [68–72]). Thus, the capacitance associated with the diffusion region will be much smaller than the total capacitance of the EISCAP used in our experiments. For this reason, in a simplified capacitive model, to a first approximation, we neglected the possible influence of lateral diffusion of the produced protons from the enzyme-covered to the enzyme-free region.

Unfortunately, the multicell utilized in this study is not suited for the experimental investigation of an influence of the lateral diffusion of produced H^+ or OH^- ions on the obtained results. On the other hand, the multicell setup allows to measure possible pH changes in the bulk solution, resulting from the diffusion of H^+ or OH^- ions in the direction perpendicular to the EISCAP surface (instead of a lateral diffusion). Therefore, we have performed additional experiments to measure pH changes in the perpendicular direction induced by the penicillinase/penicillin reaction. For this, a commercial pH electrode (InLab Micro Pro-ISM, Mettler-Toledo, Germany) was positioned over a single penicillinase-immobilized EISCAP surface at a distance of about ≤ 1 mm from the sensor surface, and the pH value was recorded in a 1 mM penicillin solution for about 20 min. The registered pH change after 20 min measurement was 0.11 pH that corresponds only to approximately 7% of the surface pH change of $\Delta pH \approx 1.6$, estimated from the ConCap measurements in Fig. 4d. Based on the results of these experiments and by assuming that the diffusion length in the direction perpendicular to the EISCAP surface and the lateral diffusion length are comparable, it can be concluded that the lateral diffusion of H^+ ions will have an insignificant impact on the obtained results. The lateral diffusion of H^+ ions will reduce to some extent the enzyme-free passive surface area, where the surface potential remains unchanged. However, the main findings of this study – an increase of the enzyme coverage enhances the EISCAP signal and the analyte sensitivity of the biosensor – will remain intact. Nonetheless, in future works, the impact of the lateral diffusion of produced ions will be investigated in more detail by using a modified EISCAP structure and a novel design of the measurement cell.

4.3. Towards multianalyte detection with a multi-enzyme modified EISCAP

As outlined in the Introduction, the design of an array of separate EISCAPs on the same chip for multiplexed sensing of different species, without mutual interference between the different EISCAPs, is challenging and requires complex fabrication technologies. In principle, an EISCAP biosensor for multianalyte detection can be accomplished by immobilizing different receptor molecules on different spots of the single EISCAP surface. However, in such configuration the capacitive field-effect structures underneath these sensitive regions will be interconnected through the common silicon substrate. Accordingly, the overall capacitance of the single EISCAP will be determined by parallel-connected capacitances of EISCAP regions, corresponding to surface areas immobilized with different receptors: The resulting cross-talk will hinder the selective detection of a particular target analyte in the multianalyte solution. As an alternative, a single EISCAP functionalized with various enzymes can be used to detect multiple analytes in a sequential manner via consecutive exchange of samples spiked with the respective target analyte; this will be demonstrated experimentally below. The price to be paid, however, will be a smaller signal amplitude and therefore, a lower analyte sensitivity.

For these experiments, the two model enzymes penicillinase and urease were selected for the detection of penicillin and urea. Eight EISCAPs (EISCAPs 1–4 and 9–12) in the multicell were immobilized with penicillinase, while the remaining eight EISCAPs (EISCAPs 5–8 and 13–16) were immobilized with urease (see Fig. 6a, left). To demonstrate the ability of EISCAPs for multianalyte detection, the sixteen EISCAPs in the multicell were divided again into four groups (A, B, C, and D), each combining two penicillinase- and two urease-functionalized individual EISCAPs. All four EISCAPs of each group were electrically connected in parallel, thus mimicking an EISCAP with an active surface area that is divided into two equal spots. This situation corresponds to an EISCAP with a surface coverage $\eta = 0.5$ or 50% for both enzymes, which will detect the two analytes (penicillin and urea) sequentially.

Fig. 6a (right) exemplarily depicts normalized ConCap signals for four parallel-connected EISCAPs in groups A, B, C and D, recorded in buffer and in 1 mM urea or 1 mM penicillin solution, respectively. Evidently, in the presence of 1 mM urea solution (minute 10–20), the ConCap response of four parallel-connected EISCAPs in all groups shifts in the direction to positive voltages by 33 – 43 mV. This change of the ConCap signals corresponds to a more negatively charged gate surface and can be attributed to the local pH increase near the Ta_2O_5 surface of the urease-modified EISCAPs induced by the enzymatic urease/urea reaction. This means that OH^- ions are produced, according to the following reaction scheme [7,73,74]:

$$\text{urea} + 3H_2O \xrightarrow{urease} CO_2 + 2NH_4^+ + 2OH^- \quad (15)$$

After the second measurement of the ConCap signals in buffer solution (minute 20–30), the EISCAPs were exposed to 1 mM penicillin solution (minute 30–40). In contrast to the measurement in urea solution, the ConCap responses of four parallel-connected EISCAPs in all groups shift towards more negative voltages, which corresponds to a more positively charged gate surface. Since four parallel-connected EISCAPs combine two urease- and two penicillinase-modified sensors, the ConCap signal shifts towards negative voltages can be attributed to the locally increased proton concentration (i.e., pH decrease) close to the Ta_2O_5 surface of the penicillinase-covered EISCAPs caused by the penicillinase/penicillin enzymatic reaction (as discussed in Section 4.2). The amplitude of the recorded signal shift (56 – 58 mV) was consistent with the results obtained in Fig. 4d for a penicillinase coverage of $\eta = 0.5$ (58 mV) and approximately 1.6 times smaller than that of a single or parallel-connected EISCAPs with a penicillinase coverage of $\eta = 1$ (93 mV).

Finally, we studied whether the possible lateral diffusion of H^+ or OH^- ions generated by the enzymatic reactions could provoke cross-talk effects between neighboring EISCAPs in the multicell. Therefore, four penicillinase-immobilized EISCAPs in group A (EISCAPs 1 – 4) and group C (EISCAPs 9 – 12) as well as four urease-immobilized EISCAPs in group B (EISCAPs 5 – 8) and group D (EISCAPs 13 – 16) were connected in parallel (see Fig. 6b, left). They mimic penicillin- or urea-sensitive EISCAPs with a penicillinase or urease coverage of $\eta = 1$ (i.e., 100%). The results of these experiments are displayed in Fig. 6b, right. First, the ConCap signal of parallel-connected EISCAPs immobilized with urease or penicillinase were recorded in buffer (minute 0–10) and then in 1 mM urea solution (minute 10–20). As can be seen, the presence of 1 mM urea in the solution results in a ConCap-signal change of urease-immobilized EISCAPs by about 89 – 96 mV in the direction to positive voltages. In contrast, negligible changes in the ConCap signals of 6 – 8 mV were observed for the penicillinase-immobilized EISCAPs in the urea solution.

After a second measurement in buffer solution (minute 20–30), the EISCAPs were exposed to 1 mM penicillin solution (minute 30–40). Shifts in the ConCap signal of 100 – 102 mV in the direction to negative voltages were recorded for the parallel-connected penicillinase-modified EISCAPs. At the same time, as expected, registered changes in the

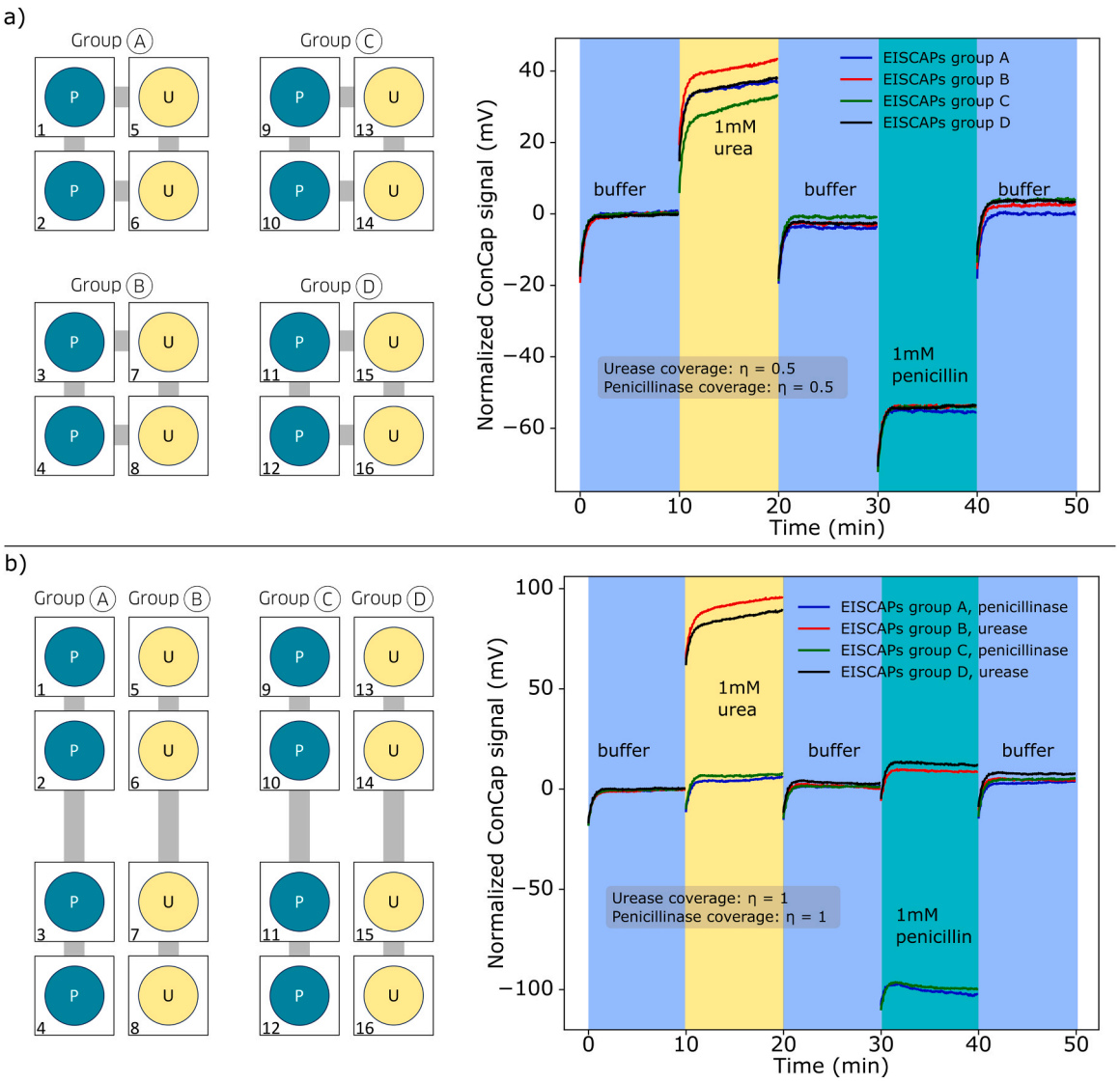

Fig. 6. (a) Combination of four parallel-connected enzyme-modified single EISCAPs in each group (A, B, C, D), mimicking a penicillinase and urease coverage of $\eta = 0.5$ (left) and corresponding normalized ConCap signals (right). b) Combination of four parallel-connected penicillinase- (groups A and C) and urease-modified (groups B and D) single EISCAPs, mimicking penicillinase and urease coverage of $\eta = 1$ (left) and normalized ConCap signals (right). The ConCap signals were recorded in buffer and in 1 mM urea or 1 mM penicillin solution. P: penicillinase; U: urease. The electrical connections are depicted as gray lines.

ConCap signals of the urease-immobilized EISCAPs in the penicillin solution were again small in the order of $8 - 9$ mV. If cross-talk would exist between neighboring EISCAPs, the ConCap signal of urease-modified EISCAPs in penicillin solution should shift towards negative voltages, which is not the case in the experiments presented in Fig. 6b (right).

To additionally check whether the diffusion of produced H^+ or OH^- ions during the multicell experiment can cause cross-talk between the EISCAPs, we estimated the time t_D required for diffusion transport of ions over the minimum distance $S \approx 13$ mm between two neighboring EISCAPs using the following expression [60,75]:

$$D = S^2/2t_D \tag{16}$$

Here, D is the diffusion coefficient of ions ($D_H = 9.33\times10^{-9}$ m^2/s and $D_{OH} = 5.21\times10^{-9}$ m^2/s at 25 °C for H^+ and OH^- ions, respectively [76]). The calculated t_D values (2.5 h for H^+ ions and 4.5 h for OH^- ions) are much longer than the ConCap measurement period (10 min), which confirms that interferences between the EISCAPs in the multicell are indeed absent.

The obtained findings reveal the capability of EISCAPs covered with multi-enzymes to detect multiple analytes in a sequential manner by exchanging the measurement solutions spiked with the respective target analyte. In particular, EISCAPs with immobilized penicillinase and urease can be used for the detection of penicillin in solutions, which do not contain urea, or for the detection of urea in solutions, which do not contain penicillin. However, in the case of presence of both substrates (i.e., penicillin and urea) in the solution, both the penicillinase- and the urease-immobilized regions are active and will contribute to the total EISCAP signal. As a consequence, such an EISCAP sensor will be unable to selectively distinguish between the target analytes in a multianalyte solution. Moreover, in the specific scenario of the penicillinase/penicillin and urease/urea system, the two enzymatic reactions will produce opposite pH changes and thus, a reduced overall EISCAP sensor signal. In some experimental conditions, even a fully compensation of signals generated by the two enzymatic reactions can be achieved, which has been used for the realization of an enzyme-based XOR (Exclusive OR) logic gate (see e.g., [33,77]).

5. Conclusions

The EISCAP represents a primary transducer structure for designing

various field-effect biochemical sensors, including enzyme biosensors. In this study, a capacitive model for an enzyme-modified EISCAP has been developed and the impact of enzyme surface coverage on the biosensor performance was studied theoretically and experimentally. To achieve different enzyme coverages, bare and enzyme-covered (penicillinase) single EISCAPs in diverse combinations were electrically connected in parallel. The utilized multicell design enabled a multiplexed electrochemical characterization of up to sixteen EISCAPs in the established $C-V$ and ConCap modes.

As predicted by the model, both the shift of the $C-V$ curve along the voltage axis and the amplitude of the ConCap signal show a clear dependence on enzyme coverage. For instance, with increasing penicillinase coverage from $\eta = 0.25$ to $\eta = 1$, the normalized ConCap signal, recorded at a penicillin concentration of 1 mM, raised from 28 mV to 93 mV. Moreover, an increase of the penicillinase coverage enhances the penicillin sensitivity of the EISCAP biosensor from 42 mV/dec at $\eta = 0.5$ to 70 mV/dec at $\eta = 1$. Lastly, the ability of the multicell arrangement with bi-enzyme (urease and penicillinase) modified EISCAPs for the sequential multianalyte (urea and penicillin) detection was experimentally demonstrated and discussed.

The theoretical model and experimental findings reveal that the enzyme surface coverage has a significant influence on the EISCAP signals and, thus, the biosensor performance. Therefore, this effect should be taken into account by designing enzyme-based field-effect biosensors as well as by comparison of their performances. The model presented in this study could be adapted to various types of enzyme-modified field-effect biosensors.

CRediT authorship contribution statement

Stefan Achtsnicht: Validation, Formal analysis, Conceptualization. **Patrick Wagner:** Writing – review & editing, Validation, Supervision. **Michael J. Schoening:** Writing – review & editing, Writing – original draft, Visualization, Validation, Supervision, Resources, Methodology, Conceptualization. **Tobias Karschuck:** Writing – review & editing, Writing – original draft, Visualization, Methodology, Investigation. **Arshak Poghossian:** Writing – original draft, Methodology, Investigation, Formal analysis, Conceptualization. **Joey Ser:** Methodology, Investigation. **Astghik Tsokolakyan:** Methodology, Investigation.

Declaration of Competing Interest

The authors declare that they have no known competing financial interests or personal relationships that could have appeared to influence the work reported in this paper.

Data availability

Data will be made available on request.

Acknowledgements

The authors would like to thank S. Schmidt, M. Welden and M. Yeranosyan for valuable discussions. Part of this work was supported by the Deutsche Forschungsgemeinschaft (DFG, German Research Foundation, grant 445454801). Part of this work was supported by the MoESCS RA (22AA-2J02 and 22-YSIP-041).

Appendix A. Supporting information

Supplementary data associated with this article can be found in the online version at doi:10.1016/j.snb.2024.135530.

References

[1] S. Cao, P. Sun, G. Xiao, Q. Tang, X. Sun, H. Zhao, S. Zhao, H. Lu, Z. Yue, ISFET-based sensors for (bio)chemical applications: a review, Electrochem. Sci. Adv. 3 (2023) e2100207, https://doi.org/10.1002/elsa.202100207.
[2] L. Sarcina, E. Macchia, A. Tricase, C. Scandurra, A. Imbriano, F. Torricelli, N. Cioffi, L. Torsi, P. Bollella, Enzyme based field effect transistor: state-of-the-art and future perspectives, Electrochem. Sci. Adv. 3 (2023) e2100216, https://doi.org/10.1002/elsa.202100216.
[3] C.-A. Vu, W.-Y. Chen, Field-effect transistor biosensors for biomedical applications: recent advances and future prospects, Sensors 19 (2019) 4214, https://doi.org/10.3390/s19194214.
[4] A. de Moraes, L. Kubota, Recent trends in field-effect transistors-based immunosensors, Chemosensors 4 (2016) 20, https://doi.org/10.3390/chemosensors4040020.
[5] T. Sakata, Biologically coupled gate field-effect transistors meet in vitro diagnostics, ACS Omega 4 (2019) 11852–11862, https://doi.org/10.1021/acsomega.9b01629.
[6] A. Poghossian, M.J. Schöning, Recent progress in silicon-based biologically sensitive field-effect devices, Curr. Opin. Electrochem. 29 (2021) 100811, https://doi.org/10.1016/j.coelec.2021.100811.
[7] A. Poghossian, M.J. Schöning, Capacitive field-effect EIS chemical sensors and biosensors: a status report, Sensors 20 (2020) 5639, https://doi.org/10.3390/s20195639.
[8] M. Chen, Y. Jin, X. Qu, Q. Jin, J. Zhao, Electrochemical impedance spectroscopy study of Ta_2O_5 based EIOS pH sensors in acid environment, Sens. Act. B: Chem. 192 (2014) 399–405, https://doi.org/10.1016/j.snb.2013.10.129.
[9] D. Molinnus, H. Iken, A.L. Johnen, B. Richstein, L. Hellmich, A. Poghossian, J. Knoch, M.J. Schöning, Miniaturized pH-sensitive field-effect capacitors with ultrathin Ta_2O_5 films prepared by atomic layer deposition, Phys. Stat. Sol. (a) 219 (2022) 2100660, https://doi.org/10.1002/pssa.202100660.
[10] Y. Mourzina, T. Mai, A. Poghossian, Y. Ermolenko, T. Yoshinobu, Y. Vlasov, H. Iwasaki, M. J. Schöning, K^+-selective field-effect sensors as transducers for bioelectronic applications, Electrochim. Acta 48 (2003) 3333–3339, https://doi.org/10.1016/S0013-4686(03)00402-X.
[11] H. Cho, K. Kim, M. Meyyappan, C.-K. Baek, LaF_3 electrolyte-insulator-semiconductor sensor for detecting fluoride ions, Sens. Act. B Chem. 279 (2019) 183–188, https://doi.org/10.1016/j.snb.2018.09.094.
[12] E.M. Al-Khalqi, M.A. Abdul Hamid, N.H. Al-Hardan, L.K. Keng, A. Jalar, Magnesium-doped ZnO nanorod electrolyte-insulator-semiconductor (EIS) sensor for detecting calcium ions, J. Mater. Sci.: Mater. Electron. 33 (2022) 1618–1630, https://doi.org/10.1007/s10854-022-07696-x.
[13] Y.-R. Ye, J.-C. Wang, Y.-T. Chan, Anion sensing and interfering behaviors of electrolyte-insulator-semiconductor sensors with nitrogen plasma-treated samarium oxide, Jpn. J. Appl. Phys. 54 (2015) 04DL04, https://doi.org/10.7567/JJAP.54.04DL04.
[14] T.-M. Pan, T.-W. Lin, C.-Y. Chen, Label-free detection of rheumatoid factor using YbYxOy electrolyte-insulator-semiconductor devices, Anal. Chim. Acta 891 (2015) 304–311, https://doi.org/10.1016/j.aca.2015.08.014.
[15] H. Hlukhova, M. Menger, A. Offenhäusser, S. Vitusevich, Highly sensitive aptamer-based method for the detection of cardiac biomolecules on silicon dioxide surfaces, MRS Adv. 3 (2018) 1535–1541, https://doi.org/10.1557/adv.2018.332.
[16] M. Bahri, A. Baraket, N. Zine, M. Ben Ali, J. Bausells, A. Errachid, Capacitance electrochemical biosensor based on silicon nitride transducer for TNF-α cytokine detection in artificial human saliva: heart failure (HF), Talanta 209 (2020) 120501, https://doi.org/10.1016/j.talanta.2019.120501.
[17] T.S. Bronder, A. Poghossian, M.P. Jessing, M. Keusgen, M.J. Schöning, Surface regeneration and reusability of label-free DNA biosensors based on weak polyelectrolyte-modified capacitive field-effect structures, Biosens. Bioelectron. 126 (2019) 510–517, https://doi.org/10.1016/j.bios.2018.11.019.
[18] T.-M. Pan, K.-Y. Chang, C.-W. Lin, S.-W. Tsai, M.-H. Wu, Label-free detection ofDNA using high-κ$Lu_2Ti_2O_7$ electrolyte-insulator-semiconductors, J. Mater. Chem. 22 (2012) 1358–1363, https://doi.org/10.1039/C1JM14274G.
[19] N. Kumar, S. Kumar, J. Kumar, S. Panda, Investigation of mechanisms involved in the enhanced label free detection of prostate cancer biomarkers using field effect devices, J. Electrochem. Soc. 164 (2017) B409–B416, https://doi.org/10.1149/2.0541709jes.
[20] R. Chand, D. Han, S. Neethirajan, Y.-S. Kim, Detection of protein kinase using an aptamer on a microchip integrated electrolyte-insulator-semiconductor sensor, Sens. Act. B Chem. 248 (2017) 973–979, https://doi.org/10.1016/j.snb.2017.02.140.
[21] M. Jablonski, A. Poghossian, R. Severins, M. Keusgen, C. Wege, M.J. Schöning, Capacitive field-effect biosensor studying adsorption of tobacco mosaic virus particles, Micromachines 12 (2021) 57, https://doi.org/10.3390/mi12010057.
[22] M. Jablonski, A. Poghossian, M. Keusgen, C. Wege, M.J. Schöning, Detection of plant virus particles with a capacitive field-effect sensor, Anal. Bioanal. Chem. 413 (2021) 5669–5678, https://doi.org/10.1007/s00216-021-03448-8.
[23] A. Poghossian, M. Jablonski, D. Molinnus, C. Wege, M.J. Schöning, Field-effect sensors for virus detection: from Ebola to SARS-CoV-2 and plant viral enhancers, Front. Plant. Sci. 11 (2020) 598103, https://doi.org/10.3389/fpls.2020.598103.
[24] A. Poghossian, M. Bäcker, D. Mayer, M.J. Schöning, Gating capacitive field-effect sensors by the charge of nanoparticle/molecule hybrids, Nanoscale 7 (2015) 1023–1031, https://doi.org/10.1039/c4nr05987e.
[25] T. Karschuck, C. Kaulen, A. Poghossian, P.H. Wagner, M.J. Schöning, Gold nanoparticle-modified capacitive field-effect sensors: studying the surface density of nanoparticles and coupling of charged polyelectrolyte macromolecules,

Electrochem. Sci. Adv. 2 (2022) e2100179, https://doi.org/10.1002/elsa.202100179.
[26] A. Poghossian, T. Karschuck, P. Wagner, M.J. Schöning, Field-effect capacitors decorated with ligand-stabilized gold nanoparticles: modeling and experiments, Biosensors 12 (2022) 334, https://doi.org/10.3390/bios12050334.
[27] S. Schusser, M. Krischer, M. Bäcker, A. Poghossian, P. Wagner, M.J. Schöning, Monitoring of the enzymatically catalyzed degradation of biodegradable polymers by means of capacitive field-effect sensors, Anal. Chem. 87 (2015) 6607–6613, https://doi.org/10.1021/acs.analchem.5b00617.
[28] G.Z. Garyfallou, L.C. de Smet, E.J. Sudhölter, The effect of the type of doping on the electrical characteristics of electrolyte–oxide–silicon sensors: pH sensing and polyelectrolyte adsorption, Sens. Act. B: Chem. 168 (2012) 207–213, https://doi.org/10.1016/j.snb.2012.04.010.
[29] A. Poghossian, M. Weil, A.G. Cherstvy, M.J. Schöning, Electrical monitoring of polyelectrolyte multilayer formation by means of capacitive field-effect devices, Anal. Bioanal. Chem. 405 (2013) 6425–6436, https://doi.org/10.1007/s00216-013-6951-9.
[30] T.-M. Pan, C.-W. Lin, High-κ Dy_2TiO_5 electrolyte-insulator-semiconductor urea biosensors, J. Electrochem. Soc. 158 (2011) J100, https://doi.org/10.1149/1.3547723.
[31] C.F. Lin, C.H. Kao, C.Y. Lin, K.L. Chen, Y.H. Lin, NH_3 plasma–treated magnesium doped zinc oxide in biomedical sensors with electrolyte-insulator-semiconductor (EIS) structure for urea and glucose applications, Nanomaterials 10 (2020) 583, https://doi.org/10.3390/nano10030583.
[32] D. Molinnus, S. Beging, C. Lowis, M.J. Schöning, Towards a multi-enzyme capacitive field-effect biosensor by comparative study of drop-coating and nano-spotting technique, Sensors 20 (2020) 4924, https://doi.org/10.3390/s20174924.
[33] M. Welden, A. Poghossian, F. Vahidpour, T. Wendlandt, M. Keusgen, C. Wege, M. J. Schöning, Towards multi-analyte detection with field-effect capacitors modified with tobacco mosaic virus bioparticles as enzyme nanocarriers, Biosensors 12 (2022) 43, https://doi.org/10.3390/bios12010043.
[34] Y.-H. Lin, S.-H. Wang, M.-H. Wu, T.-M. Pan, C.-S. Lai, J.-D. Luo, C.-C. Chiou, Integrating solid-state sensor and microfluidic devices for glucose, urea and creatinine detection based on enzyme-carrying alginate microbeads, Biosens. Bioelectron. 43 (2013) 328–335, https://doi.org/10.1016/j.bios.2012.12.053.
[35] Y.-H. Lin, A. Das, M.-H. Wu, T.-M. Pan, C.-S. Lai, Microfluidic chip integrated with an electrolyte-insulator-semiconductor sensor for ph and glucose level measurement, Int. J. Electrochem. Sci. 8 (2013) 5886–5901, https://doi.org/10.1016/S1452-3981(23)14729-8.
[36] Y.-H. Lin, C.-H. Chiang, M.-H. Wu, T.-M. Pan, J.-D. Luo, C.-C. Chiou, Solid-state sensor incorporated in microfluidic chip and magnetic-bead enzyme immobilization approach for creatinine and glucose detection in serum, APL 99 (2011) 253704, https://doi.org/10.1063/1.3671078.
[37] T.-M. Pan, C.-W. Lin, W.-Y. Lin, M.-H. Wu, High-κ $Tm_2Ti_2O_7$ electrolyte-insulator-semiconductor creatinine biosensor, Ieee. Sens. J. 11 (2011) 2388–2394, https://doi.org/10.1109/JSEN.2011.2122255.
[38] A. Poghossian, M. Thust, M.J. Schöning, M. Müller-Veggian, P. Kordos, H. Lüth, Cross-sensitivity of a capacitive penicillin sensor combined with a diffusion barrier, Sens. Act. B: Chem. 68 (2000) 260–265, https://doi.org/10.1016/S0925-4005(00)00442-1.
[39] M.H. Abouzar, A. Poghossian, J.R. Siqueira, O.N. Oliveira, W. Moritz, M. J. Schöning, Capacitive electrolyte-insulator-semiconductor structures functionalised with a polyelectrolyte/enzyme multilayer: New strategy for enhanced field-effect biosensing, Phys. Stat. Sol. (a 207 (2010) 884–890, https://doi.org/10.1002/pssa.200983317.
[40] A. Poghossian, M. Jablonski, C. Koch, T.S. Bronder, D. Rolka, C. Wege, M. J. Schöning, Field-effect biosensor using virus particles as scaffolds for enzyme immobilization, Biosens. Bioelectron. 110 (2018) 168–174, https://doi.org/10.1016/j.bios.2018.03.036.
[41] M. Welden, A. Poghossian, F. Vahidpour, T. Wendlandt, M. Keusgen, W. Christina, M.J. Schöning, Capacitive field-effect biosensor modified with a stacked bilayer of weak polyelectrolyte and plant virus particles as enzyme nanocarriers, Bioelectrochemistry 151 (2023) 108397, https://doi.org/10.1016/j.bioelechem.2023.108397.
[42] M. Welden, R. Severins, A. Poghossian, C. Wege, J. Bongaerts, P. Siegert, M. Keusgen, M.J. Schöning, Detection of acetoin and diacetyl by a tobacco mosaic virus-assisted field-effect biosensor, Chemosensors 10 (2022) 218, https://doi.org/10.3390/chemosensors10060218.
[43] A. Poghossian, K. Malzahn, M.H. Abouzar, P. Mehndiratta, E. Katz, M.J. Schöning, Integration of biomolecular logic gates with field-effect transducers, Electrochim. Acta 56 (2011) 9661–9665, https://doi.org/10.1016/j.electacta.2011.01.102.
[44] F. Moseley, J. Halámek, F. Kramer, A. Poghossian, M.J. Schöning, E. Katz, An enzyme-based reversible CNOT logic gate realized in a flow system, Analyst 139 (2014) 1839–1842, https://doi.org/10.1039/c4an00133h.
[45] E. Katz, A. Poghossian, M.J. Schöning, Enzyme-based logic gates and circuits-analytical applications and interfacing with electronics, Anal. Bioanal. Chem. 409 (2017) 81–94, https://doi.org/10.1007/s00216-016-0079-7.
[46] M. Taing, D. Sweatman, Fabrication techniques for an arrayed EIS biosensor, 11th Electron. Pack. Tech. Conf. (2009) 168–173, https://doi.org/10.1109/EPTC.2009.5416557.
[47] M.H. Abouzar, A. Poghossian, A.M. Pedraza, D. Gandhi, S. Ingebrandt, W. Moritz, M.J. Schöning, An array of field-effect nanoplate SOI capacitors for (bio-)chemical sensing, Biosens. Bioelectron. 26 (2011) 3023–3028, https://doi.org/10.1016/j.bios.2010.12.006.
[48] S. Dastidar, A. Agarwal, N. Kumar, V. Bal, S. Panda, Sensitivity enhancement of electrolyte-insulator-semiconductor sensors using mesotextured and nanotextured dielectric surfaces, Ieee. Sens. J. 15 (2015) 2039–2045, https://doi.org/10.1109/JSEN.2014.2369739.
[49] B. Gil Rosa, O.E. Akingbade, X. Guo, L. Gonzalez-Macia, M.A. Crone, L.P. Cameron, P. Freemont, K.-L. Choy, F. Güder, E. Yeatman, D.J. Sharp, B. Li, Multiplexed immunosensors for point-of-care diagnostic applications, Biosens. Bioelectron. 203 (2022) 114050, https://doi.org/10.1016/j.bios.2022.114050.
[50] A. Poghossian, R. Welden, V.V. Buniatyan, M.J. Schöning, An array of on-chip integrated, individually addressable capacitive field-effect sensors with control gate: design and modelling, Sensors 21 (2021) 6161, https://doi.org/10.3390/s21186161.
[51] M. Klein, Characterization of ion-sensitive layer systems with a C(V) measurement method operating at constant capacitance, Sens. Act. B: Chem. 1 (1990) 354–356, https://doi.org/10.1016/0925-4005(90)80229-S.
[52] W.M. Siu, R. Cobbold, Basic properties of the electrolyte-SiO_2-Si system: physical and theoretical aspects, IEEE Trans. Electron. Dev. 26 (1979) 1805–1815, https://doi.org/10.1109/T-ED.1979.19690.
[53] P. Fabry, L. Laurent-Yvonnou, The C-V method for characterizing ISFET or EOS devices with ion-sensitive membranes, J. Electroanal. Chem. 286 (1990) 23–40, https://doi.org/10.1016/0022-0728(90)85062-A.
[54] S.M. Sze, K.K. Ng, Physics of Semiconductor Devices, John Wiley & Sons, 2007.
[55] P. Bergveld, Thirty years of ISFETOLOGY, Sens. Act. B: Chem. 88 (2003) 1–20, https://doi.org/10.1016/S0925-4005(02)00301-5.
[56] P. Georgiou, C. Toumazou, CMOS-based programmable gate ISFET, Electron. Lett. 44 (2008) 1289, https://doi.org/10.1049/el:20082268.
[57] P. Pookaiyaudom, F.J. Lidgey, K. Hayatleh, P. Seelanan, C. Toumazou, Chemical current conveyor (CCCII+): system design and verification for buffer index/capacity measurement, Sens. Act. B: Chem. 147 (2010) 228–233, https://doi.org/10.1016/j.snb.2010.03.037.
[58] J.R. Siqueira, R.M. Maki, F.V. Paulovich, C.F. Werner, A. Poghossian, M.C.F. de Oliveira, V. Zucolotto, O.N. Oliveira, M.J. Schöning, Use of information visualization methods eliminating cross talk in multiple sensing units investigated for a light-addressable potentiometric sensor, Anal. Chem. 82 (2010) 61–65, https://doi.org/10.1021/ac9024076.
[59] A. Poghossian, H. Lüth, J. Schultze, M. Schöning, (Bio-)chemical and physical microsensor arrays using an identical transducer principle, Electrochim. Acta 47 (2001) 243–249, https://doi.org/10.1016/S0013-4686(01)00562-X.
[60] A. Poghossian, J.W. Schultze, M.J. Schöning, Multi-parameter detection of (bio-) chemical and physical quantities using an identical transducer principle, Sens. Act. B: Chem. 91 (2003) 83–91, https://doi.org/10.1016/S0925-4005(03)00070-4.
[61] Zahner Elektrik, 2022, ⟨https://github.com/Zahner-elektrik/Thales-Remote-Python⟩(accessed January, 2022), Thales Remote Python.
[62] T. Karschuck, S. Schmidt, S. Achtsnicht, A. Poghossian, P. Wagner, M.J. Schöning, Multiplexing system for automated characterization of a capacitive field-effect sensor array, Phys. Stat. Sol. (a (2023) 2300265, https://doi.org/10.1002/pssa.202300265.
[63] T. Sawai, K. Morioka, M. Ogawa, S. Yamagishi, Inducible oxacillin-hydrolyzing penicillinase in Aeromonas hydrophila isolated from fish, Antimicrob. Agents Chemother. 10 (1976) 191–195, https://doi.org/10.1128/aac.10.2.191.
[64] S.D. Cesareo, S.R. Langton, Kinetic properties of *Helicobacter pylori* urease compared with jack bean urease, FEMS Microbiol. Lett. 99 (1992) 15–21, https://doi.org/10.1111/j.1574-6968.1992.tb05535.x.
[65] B. Veigas, R. Branquinho, J.V. Pinto, P.J. Wojcik, R. Martins, E. Fortunato, P. V. Baptista, Ion sensing (EIS) real-time quantitative monitorization of isothermal DNA amplification, Biosens. Bioelectron. 52 (2014) 50–55, https://doi.org/10.1016/j.bios.2013.08.029.
[66] S. Mross, T. Zimmermann, N. Winkin, M. Kraft, H. Vogt, Integrated multi-sensor system for parallel in-situ monitoring of cell nutrients, metabolites, cell density and pH in biotechnological processes, Sens. Act. B: Chem. 236 (2016) 937–946, https://doi.org/10.1016/j.snb.2016.03.086.
[67] A. Poghossian, A. Baade, H. Emons, M.J. Schöning, Application of ISFETs for pH measurement in rain droplets, Sens. Act. B Chem. 76 (2001) 634–638, https://doi.org/10.1016/S0925-4005(01)00659-1.
[68] T. Yoshinibu, T. Harada, H. Iwasaki, Application of the pH–imaging sensor to determining the diffusion coefficients of ions in electrolytic solutions, Jpn. J. Appl. Phys. 39 (2000) L318–L320, https://doi.org/10.1143/JJAP.39.L318.
[69] P. Temple-Boyer, J. Le Gal, M.L. Pourciel-Gouzy, W. Sant, A. Martinez, Modelling of EnFETs for the creatinine detection, Sens. Act. B: Chem. 118 (2006) 47–52, https://doi.org/10.1016/j.snb.2006.04.011.
[70] P. Temple-Boyer, A. Benyahia, W. Sant, M.L. Pourciel-Gouzy, J. Launay, A. Martinez, Modelling of urea-EnFETs for haemodialysis applications, Sens. Act. B: Chem. 131 (2008) 525–532, https://doi.org/10.1016/j.snb.2007.12.037.
[71] J. Suzurikawa, M. Nakao, R. Kanzaki, H. Takahashi, Microscale pH gradient generation by electrolysis on a light-addressable planar electrode, Sens. Act. B: Chem. 149 (2010) 205–211, https://doi.org/10.1016/j.snb.2010.05.058.
[72] R. Welden, M. Jablonski, C. Wege, M. Keusgen, P.H. Wagner, T. Wagner, M. J. Schöning, Light-addressable actuator-sensor platform for monitoring and manipulation of pH gradients in microfluidics: a case study with the enzyme penicillinase, Biosensors 11 (2021) 171, https://doi.org/10.3390/bios11060171.
[73] C.-E. Lue, T.-C. Yu, C.-M. Yang, D.G. Pijanowska, C.-S. Lai, Optimization of urea-EnFET based on Ta_2O_5 layer with post annealing, Sensors 11 (2011) 4562–4571, https://doi.org/10.3390/s110504562.
[74] N.C. Vieira, A. Figueiredo, E.G. Fernandes, F.E. Guimarães, V. Zucolotto, Nanostructured polyaniline thin films as urea-sensing membranes in field-effect devices, Synth. Met. 175 (2013) 108–111, https://doi.org/10.1016/j.synthmet.2013.05.005.

[75] A.J. Bard, L.R. Faulkner, Electrochemical Methods, Fundamentals and Applications, Wiley, 1980.
[76] W. Olthuis, J.G. Bomer, P. Bergveld, M. Bos, W.E. van der Linden, Iridium oxide as actuator material for the ISFET-based sensor-actuator system, Sens. Act. B Chem. 5 (1991) 47–52, https://doi.org/10.1016/0925-4005(91)80218-9.
[77] M. Jablonski, A. Poghossian, D. Molinnus, M. Keusgen, E. Katz, M.J. Schöning, Enzyme-based XOR logic gate with electronic transduction of the output signal, Int. J. Unconv. Comput. 14 (2019) 375–383.

Tobias Karschuck studied biomedical engineering at Aachen University of Applied Sciences. He received his MSc degree in 2021. Following, he started his Ph.D. thesis at the Institute of Nano- and Biotechnologies (INB) at the Aachen University of Applied Sciences in collaboration with the Laboratory of Soft Matter and Biophysics at KU Leuven. His main research interests concern nanoparticle-modified field-effect sensors for biomarker detection.

Arshak Poghossian received his PhD degree in solid-state physics from Leningrad Electrotechnic Institute in 1978 and the Dr. Sci. degree in solid-state electronics and microelectronics from the State University of Yerevan (Armenia) in 1995. After being an associate professor of State Engineering University of Armenia and director of Microsensor Ltd. (Yerevan) from 1991 to 1996, he has been a professor at the University of Management and Information (Yerevan). Since 1998, he has been with the Institute of Thin Films and Interfaces at the Research Centre Jülich, and from 2004 until 2018, he joined the Institute of Nano- and Biotechnologies (INB) at Aachen University of Applied Sciences, Germany. In 2008, he has been appointed as Honorary Professor. In 2011, he was elected as a Foreign Member of the Armenian National Academy of Sciences. In 2019, he founded the company MicroNanoBio. His research interests are solid-state chemical sensors and biosensors, sensor materials, nano-devices, microsystem technology, nano- and biotechnology.

Joey Ser is currently studying for her BEng degree at Aachen University of Applied Sciences. Her research interest focuses on the functionalization of capacitive field-effect sensors with enzymes and antibodies.

Astghik Tsokolakyan studied membrane engineering in the Erasmus Mundus master program (EM^3E–^4SW) and received an MSc degree in 2020. She started her Ph.D. thesis in ICNT at the Institute of Chemical Physics, NAS RA. Her research interests are the development and characterization of optical and capacitive biosensors decorated with nanoparticles.

Stefan Achtsnicht obtained a Ph.D. in physics in 2020 at RWTH Aachen University in the field of magnetic detection of superparamagnetic beads. He is currently working as a postdoctoral researcher at Aachen University of Applied Sciences in the Institute of Nano- and Biotechnologies (INB). His research interests include frequency mixing magnetic detection, biodegradable biosensors, silicon-based chemical and biosensors and sensor-based solutions to monitor gaseous sterilization processes.

Patrick Wagner obtained a Ph.D. in physics in 1994 at Technical University Darmstadt and did postdoctoral research on the magneto-transport properties of perovskites at KU Leuven between 1995 and 2001. In 2001, he became a professor for experimental biophysics at Hasselt University and in 2014 he returned to KU Leuven as a full professor for the physics of biofunctional surfaces. P. Wagner received several grants and distinctions, was president of the Belgian Physical Society (2006–2007), and serves currently as an editor-in-chief of the Elsevier journal Physics in Medicine.

Michael J. Schöning received his Ph.D. (1993) at Karlsruhe University of Technology in the field of semiconductor-based microsensors for ion detection in liquids. From 1993–1999, he has been with the Institute of Thin Films and Interfaces (now, Institute of Biological Information Processing) at Research Center Jülich. In 1999, he was appointed as full Professor at Aachen University of Applied Sciences, Campus Jülich. Since 2006, he serves as director of the Institute of Nano- and Biotechnologies (INB) at Aachen University of Applied Sciences. His main research subjects concern silicon-based chemical and biosensors, thin-film technologies, solid-state physics, microsystem and nano(bio-) technology.